Zuse Institute Berlin

Takustr. 7
14195 Berlin
Germany

ARTHUR STRAUBE, STEFANIE WINKELMANN,
FELIX HÖFLING

Accurate reduced models for the pH oscillations in the urea-urease reaction confined to giant lipid vesicles

ZIB Report 22-21 (11 2022)

Zuse Institute Berlin
Takustr. 7
14195 Berlin
Germany

Telephone: +49 30 84185-0
Telefax: +49 30 84185-125

E-mail: bibliothek@zib.de
URL: http://www.zib.de

ZIB-Report (Print) ISSN 1438-0064
ZIB-Report (Internet) ISSN 2192-7782

Accurate Reduced Models for the pH Oscillations in the Urea–Urease Reaction Confined to Giant Lipid Vesicles

Arthur V. Straube,[*,†] Stefanie Winkelmann,[†] and Felix Höfling[‡,†]

†*Zuse Institute Berlin, Takustraße 7, 14195 Berlin, Germany*

‡*Freie Universität Berlin, Department of Mathematics and Computer Science, Arnimallee 6, 14195 Berlin, Germany*

E-mail: straube@zib.de

Abstract

Our theoretical study concerns an urea-urease-based pH oscillator confined to giant lipid vesicles. Under suitable conditions, differential transport of urea and hydrogen ion across the unilamellar vesicle membrane periodically resets the pH clock that switches the system from acid to basic, resulting in self-sustained oscillations. We analyse the structure of the limit cycle, which controls the dynamics for giant vesicles and dominates the strongly stochastic oscillations in small vesicles of submicrometer size. To this end, we derive reduced models, amenable to analytic treatments, and show that the accuracy of predictions, including the period of oscillations, is highly sensitive to the choice of the reduction scheme. In particular, we suggest an accurate two-variable model and show its equivalence to a three-variable model that admits an interpretation in terms of a chemical reaction network. The accurate description of a single pH oscillator appears crucial for rationalizing experiments and understanding communication of vesicles and synchronization of rhythms.

Graphical TOC Entry

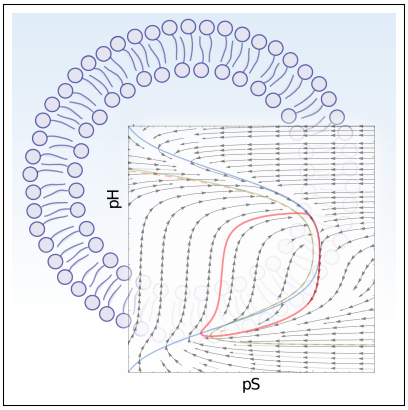

Introduction

Recent years have seen a growing surge of interest in design and development of chemical oscillators for applications.[1–3] Both in natural intracellular environments and under engineered *in vitro* conditions, the enzyme-assisted reaction kinetics is typically confined to small vesicles, i.e., permeable membrane-based micro- to nano-sized compartments.[4] The concentration of the hydrogen ion, H^+, or, equivalently, the level of pH is an important factor that controls the speed of enzymatic reactions.[5] Systems in which the hydrogen ion plays the central role and causes self-sustained oscillatory behavior belong to the class of pH oscillators.[2] Many examples of pH oscillations result from an interplay of chemical reactions that involve positive and negative feedback and occur in closed reactors. In contrast to the conventional systems, we discuss here a different mechanism of pH oscillations that relies on an open reactor.

Motivated by experimental implementations[6,7] and direct relevance for applications,[8–10] we consider an urea-urease-based pH oscillator confined to a lipid vesicle as an open reactor. Ureases are a group of enzymes for the hydrolysis of urea,[11] which occur widely in the cytoplasm of bacteria, invertebrates, fungi, and plants, but also in soils. The activity of urease is highly sensitive to the pH level and is maximal in a pH-neutral environment.[11–14] This renders the urea–urease reaction a typical pH clock that switches the system from acid to basic.[6,15] The clock can be "reset" if one allows for the exchange of acid and urea with an external reservoir such that the initial concentrations are recovered, thereby completing the elementary cycle of the oscillator. One potential realization of such a pH oscillator makes use of differential transport of hydrogen ion and urea across lipid vesicle membranes:[16] placing the vesicles in a suitable urea and pH buffer leads to a recovery of the internal concentrations and thus periodic rhythms.

We have recently studied the impact of intrinsic noise on pH oscillations,[17] which becomes progressively important upon decreasing the vesicle size. It was found that the discrete nature of molecules induces a significant statistical variation of the oscillation period in small,

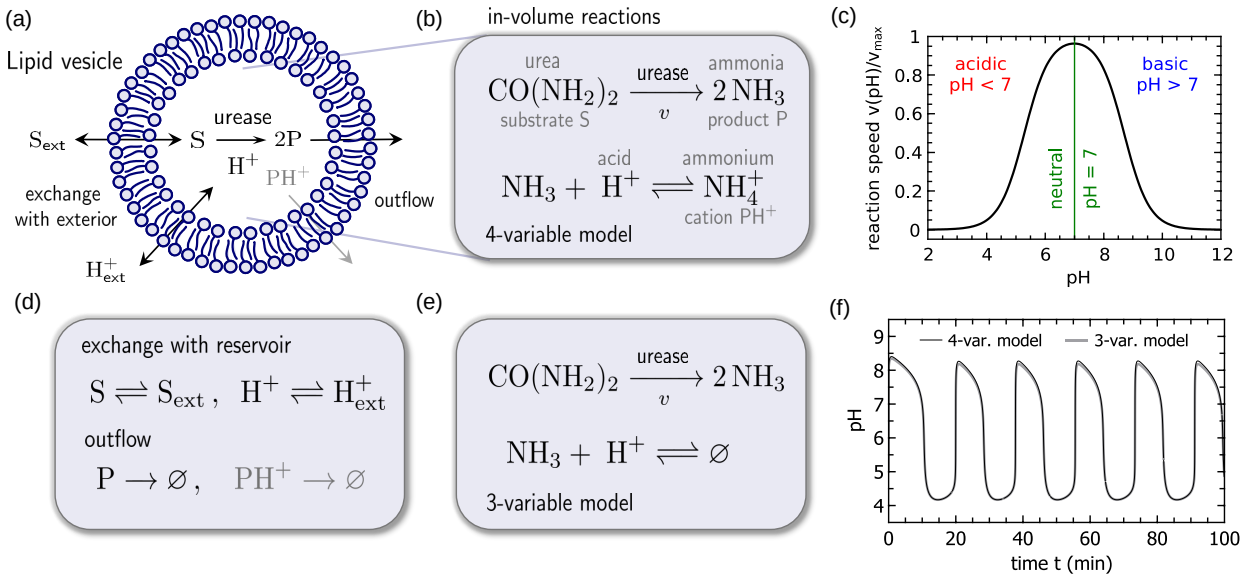

Figure 1: Schematic of the full four-variable and reduced three-variable reaction networks. (a) The enzyme (urease) assists conversion of the substrate S (urea) into product P (ammonia) in a lipid vesicle affected by varying acidity (hydrogen ion, H^+). The substrate S and acid H^+ exchange with the exterior of the vesicle, whereas the products P and PH^+ (ammonium) are subjected to outflow from the vesicle (a,d); the ion form of product PH^+ (reaction shown in gray) belongs only to the full reaction network. Volume reactions of the full, Eq. (1), (b) and reduced, Eq. (10), (e) networks occurring in the vesicle. (c) The reaction speed $v = k_{\rm cat}([S],[H^+])\,[S]$ of the catalytic step (1a) for urease, Eq. (2), shows a bell-shape dependence on $\mathrm{pH} = -\log_{10}([H^+]/1\,\mathrm{M})$ with the maximum in a neutral medium ($\mathrm{pH} \approx 7$). (f): pH oscillations obtained from the four- and three-variable models appear similar.

nano-sized vesicles; however, the limit cycle of the deterministic rate equations does not only control the dynamics for giant vesicles (of several micrometers in size), but dominates also the strongly stochastic oscillations in small vesicles. The goal of this work is the analysis of the structure of the phase flow and the limit cycle. To this end, we derive reduced models, amenable to analytic treatments, and show that the quality of predictions is highly sensitive to the choice of the reduction scheme. In particular, we suggest an accurate two-variable model and show its equivalence to a three-variable model that admits an interpretation in terms of a chemical reaction network.

Reaction scheme and four-variable model

We start with the four-variable model of pH oscillations in the urea-urease reaction confined to lipid vesicle applied in our earlier study[17] (Fig. 1a). The core of the reaction scheme are two reactions that occur within the reaction compartment:

$$\mathrm{S} \xrightarrow[k_{\mathrm{cat}}]{\text{urease}} 2\mathrm{P}\,, \tag{1a}$$

$$\mathrm{P} + \mathrm{H}^+ \underset{k_{2r}}{\overset{k_2}{\rightleftharpoons}} \mathrm{PH}^+\,. \tag{1b}$$

Reaction (1a) describes the enzyme-assisted hydrolysis of urea, $\mathrm{CO(NH_2)_2}$, into ammonia, $\mathrm{NH_3}$, in the following denoted as substrate S and product P, respectively. Reaction (1b) accounts for the acidity of the medium and involves reversible conversion between the product P and its ion form PH^+ (ammonium) with the corresponding rates[6,16,18] $k_2 = 4.3 \times 10^{10}\,\mathrm{M^{-1}s^{-1}}$ and $k_{2r} = 24\,\mathrm{s}^{-1}$. The effective speed $v([\mathrm{S}],[\mathrm{H}^+]) = k_{\mathrm{cat}}([\mathrm{S}],[\mathrm{H}^+])[\mathrm{S}]$ of reaction (1a) depends on the concentrations [S] and $[\mathrm{H}^+]$ of substrate and protons, respectively; or equivalently, on the level of $\mathrm{pH} = -\log_{10}([\mathrm{H}^+]/1\,\mathrm{M})$ and is modeled by the effective rate[5,13,16]

$$k_{\mathrm{cat}}([\mathrm{S}],[\mathrm{H}^+]) = k_{\mathrm{cat}}^{\mathrm{M}}([\mathrm{S}])\, f_{\mathrm{H}}([\mathrm{H}^+])\,. \tag{2}$$

The first factor describes the dependence on the substrate as captured by the Michaelis–Menten kinetics,

$$k_{\mathrm{cat}}^{\mathrm{M}}([\mathrm{S}]) = \frac{v_{\max}}{K_{\mathrm{M}} + [\mathrm{S}]} \tag{3}$$

with the Michaelis–Menten constant[6,11,16] $K_{\mathrm{M}} = 3 \times 10^{-3}\,\mathrm{M}$. This implies that the reaction speed v grows linearly with [S] at small $[\mathrm{S}] \ll K_{\mathrm{M}}$ and monotonically saturates at its maximum value $v_{\max}$ that would be attained in the absence of pH effects. The second factor

implements the bell-shaped dependence of the reaction speed on the acidity (Fig. 1c):

$$f_{\mathrm{H}}([\mathrm{H}^+]) = \frac{1}{1 + [\mathrm{H}^+]/K_{\mathrm{E1}} + K_{\mathrm{E2}}/[\mathrm{H}^+]} \tag{4}$$

with the constants[6,11,16] $K_{\mathrm{E1}} = 5 \times 10^{-6}\,\mathrm{M}$ and $K_{\mathrm{E2}} = 2 \times 10^{-9}\,\mathrm{M}$. It implies that the speed of reaction is maximum at the normal value of pH = 7, but is strongly suppressed when shifted from this optimal value to the regions of lower (acidic) or higher (base) pH.

The core reactions (1a) and (1b) are accompanied by the exchange with a reservoir and the decay of products (Fig. 1d); the reservoir acts as a buffer of substrate and pH, originally expressed by the reactions $\mathrm{S} \overset{k_{\mathrm{S}}}{\rightleftharpoons} \mathrm{S_{ext}}$ and $\mathrm{H}^+ \overset{k_{\mathrm{H}}}{\rightleftharpoons} \mathrm{H^+_{ext}}$. By assuming a sufficiently large reservoir such that the amounts of $\mathrm{S_{ext}}$ and $\mathrm{H^+_{ext}}$ are changed only marginally, we consider the reservoir concentrations as fixed values $[\mathrm{S_{ext}}]$ and $[\mathrm{H^+_{ext}}]$. The exchange reactions are then effectively replaced by

$$\mathrm{S} \underset{k_{\mathrm{S}}[\mathrm{S_{ext}}]}{\overset{k_{\mathrm{S}}}{\rightleftharpoons}} \varnothing \qquad \text{and} \qquad \mathrm{H}^+ \underset{k_{\mathrm{H}}[\mathrm{H^+_{ext}}]}{\overset{k_{\mathrm{H}}}{\rightleftharpoons}} \varnothing\,. \tag{5}$$

The formulation of the reaction scheme is completed by specifying the decay of products or their outflow out of the reaction compartment by the reactions

$$\mathrm{P} \xrightarrow{k} \varnothing \qquad \text{and} \qquad \mathrm{PH}^+ \xrightarrow{k} \varnothing\,. \tag{6}$$

The set of reaction rate equations that corresponds to reactions (1), (5) and (6) reads:

$$\frac{d[\mathrm{S}]}{dt} = -k_{\mathrm{cat}}([\mathrm{S}], [\mathrm{H}^+])[\mathrm{S}] + k_{\mathrm{S}}([\mathrm{S_{ext}}] - [\mathrm{S}])\,, \tag{7a}$$

$$\frac{d[\mathrm{H}^+]}{dt} = k_{2r}[\mathrm{PH}^+] - k_2[\mathrm{P}][\mathrm{H}^+] + k_{\mathrm{H}}([\mathrm{H^+_{ext}}] - [\mathrm{H}^+])\,, \tag{7b}$$

$$\frac{d[\mathrm{P}]}{dt} = 2k_{\mathrm{cat}}([\mathrm{S}], [\mathrm{H}^+])[\mathrm{S}] + k_{2r}[\mathrm{PH}^+] - k_2[\mathrm{P}][\mathrm{H}^+] - k[\mathrm{P}]\,, \tag{7c}$$

$$\frac{d[\mathrm{PH}^+]}{dt} = k_2[\mathrm{P}][\mathrm{H}^+] - k_{2r}[\mathrm{PH}^+] - k[\mathrm{PH}^+]\,, \tag{7d}$$

which we will refer to as four-variable model in the following.

Focusing on the oscillatory regime, we stick to the parameter values used previously.[17] Thus, the rates of urea and proton transport correspond to $k_\mathrm{S} = 1.4 \times 10^{-3}\,\mathrm{s}^{-1}$ and $k_\mathrm{H} = 9 \times 10^{-3}\,\mathrm{s}^{-1}$, respectively; the outflow rates of both products is set to $k = k_\mathrm{S}$. For the maximum speed we use the value $v_\mathrm{max} = 1.85 \times 10^{-4}\,\mathrm{M\,s}^{-1}$, which corresponds to an urea concentration of 50 U. The external concentrations are fixed to $[\mathrm{S_{ext}}] = 3.8 \times 10^{-4}\,\mathrm{M}$ and $[\mathrm{H^+_{ext}}] = 1.3 \times 10^{-4}\,\mathrm{M}$ and the initial concentrations inside the vesicle are $[\mathrm{S}]_0 = 5 \times 10^{-5}\,\mathrm{M}$ and $[\mathrm{H^+}]_0 = 10^{-5}\,\mathrm{M}$.

For these parameters, the four-variable model [Eqs. (7)] shows oscillatory behavior in the concentrations [S], [$\mathrm{H^+}$], [P] and [$\mathrm{PH^+}$] as exemplified in Fig. 2; note the logarithmic scale in panels (a) and (b). This evolution of the concentrations essentially reproduces that of the corresponding molecular populations in the large-vesicle limit, reported in Fig. 2 of Ref. 17; the periodic variation of the pH level, roughly between 3.5 and 8.5, reflects the behavior of [$\mathrm{H^+}$] and is shown in Fig. 1f. The concentrations of $\mathrm{H^+}$ and P oscillate in anti-phase over four orders of magnitude and the evolution of [S] and [$\mathrm{PH^+}$] shows the same periodic behavior, but with a much smaller amplitude, Fig. 2b.

Quasi-steady state approximation for $\mathrm{PH^+}$

Aiming at a characterization of the limit cycle of the urea–urease oscillator, we will first pursue a dimensional reduction of the dynamical system by elimination of inessential variables. Then, we will identify the actual degrees of freedom of the system and show that the dynamical system is effectively a two-dimensional one. In our previous work,[17] starting from the four-variable model [Eqs. (7)], we applied the quasi-steady-state approximation (QSSA) simultaneously to the variables [$\mathrm{PH^+}$] and [P] in an *ad hoc* fashion. Here, we follow a more general and systematic approach, yielding more accurate reduced models and, particularly, also their regimes of validity. The model reduction occurs in two steps: In the first step, we

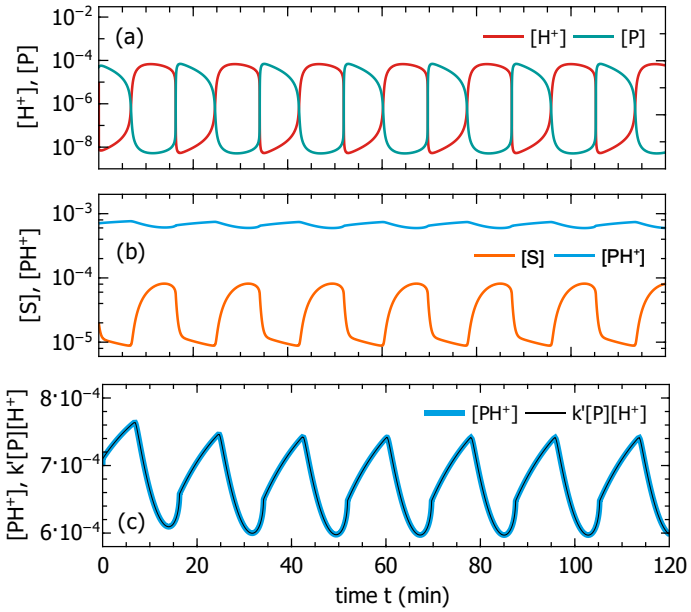

Figure 2: Evolution of concentrations showing oscillations according; numerical solution of the four-variable model, Eq. (7). (a): Concentrations $[H^+]$ (red) and [P] (turquoise). (b): Concentrations [S] (orange) and $[PH^+]$ (blue). (c): Concentration $[PH^+]$ (blue), which coincides with the combination $k'[P][H^+]$ (thin black), see Eq. (8).

eliminate $[PH^+]$, which leads to a three-variable model; this step is common to all models considered below. In the second step, we aim at a further reduction to two variables by eliminating [P], which can be performed in different ways leading to distinct models.

Reduced 3-variable model

By inspection of Fig. 2, we can draw two important conclusions. First, the concentration of the ion form of the product is larger than all other concentrations, $[PH^+] \gg [S], [H^+], [P]$. Second, the absolute variation of $[PH^+]$ is smaller than those of the other concentrations, which suggests to approximate $[PH^+](t) \approx \text{const}$, which implies $d[PH^+]/dt \approx 0$. Hence from Eq. (7d), we obtain

$$[PH^+](t) = k'\,[P](t)\,[H^+](t) = \text{const}\,, \qquad k' = \frac{k_2}{k_{2r} + k}. \tag{8}$$

This result implies that $\log([\mathrm{P}](t))$ and $\log([\mathrm{H}^+](t))$ oscillate similarly, but in antiphase, as is indeed observed in Fig. 2a. To test the quality of this approximation, we compare $[\mathrm{PH}^+(t)]$ with the product $k'[\mathrm{P}](t)[\mathrm{H}^+](t)$ graphically in Fig. 2c. We conclude that, although these quantities do not remain constant, their temporal behavior coincides at all times with high accuracy and that there exist well-separated timescales:[19,20] the fast species PH^+ adjusts quickly to the relatively slowly evolving P and H^+, which corresponds to a QSSA for PH^+ in the form $d[\mathrm{PH}^+]/dt \approx 0$. Making use of Eq. (8) in Eqs. (7b) and (7c), we arrive at a reduced model that employs only three variables:

$$\frac{d[\mathrm{S}]}{dt} = -k_{\mathrm{cat}}([\mathrm{S}],[\mathrm{H}^+])[\mathrm{S}] + k_{\mathrm{S}}([\mathrm{S}]_{\mathrm{ext}} - [\mathrm{S}])\,, \tag{9a}$$

$$\frac{d[\mathrm{H}^+]}{dt} = -kk'[\mathrm{P}][\mathrm{H}^+] + k_{\mathrm{H}}([\mathrm{H}^+]_{\mathrm{ext}} - [\mathrm{H}^+])\,, \tag{9b}$$

$$\frac{d[\mathrm{P}]}{dt} = 2k_{\mathrm{cat}}([\mathrm{S}],[\mathrm{H}^+])[\mathrm{S}] - kk'[\mathrm{P}][\mathrm{H}^+] - k[\mathrm{P}]\,. \tag{9c}$$

Note that while simplifying Eq. (9c), in accord with the above reasoning, we could have neglected the last term, $-k[\mathrm{P}]$. Indeed, the assumption $[\mathrm{PH}^+] \gg [\mathrm{P}]$ together with Eq. (8) leads to the requirement $k'[\mathrm{H}^+] \gg 1$. As independently confirmed by a previous study,[16] this is a reasonable simplification for modeling pH oscillations. However, to analyze the whole phase plane and keep the predictions of reduced models as close as possible to those of the original four-variable model, we retain this term.

The dynamic system in Eq. (9) can be interpreted as the reaction rate equations of the following effective system of in-volume reactions (Fig. 1e):

$$\mathrm{S} \xrightarrow[k_{\mathrm{cat}}]{\mathsf{urease}} 2\mathrm{P}\,, \qquad \mathrm{P} + \mathrm{H}^+ \xrightarrow{kk'} \varnothing\,. \tag{10}$$

amended by the exchange reactions (5) of S and H^+ with the reservoir and the decay of P, see the first reaction in Eq. (6) (Fig. 1d). Thus, the product P has two channels to escape from the vesicle: directly and after protonation with an effective rate. In the original reaction

scheme involving four species, the second channel exists indirectly, via escape of PH^+.

We also note that despite relation (8) is fulfilled with high accuracy, the evolutions described by the three- and four-variable models are not identical (Figs. 1f and 3). Slight quantitative differences in the predictions of the two models are visible for P and pH (and, equivalently, for $[H^+]$). Interestingly, whereas the deviations are tiny for pH, they are more pronounced for P, yet eventually less important because we are generally not interested in the dynamics of the product. What is essential is that the reduced model given by Eqs. (9) preserves not only all qualitative features of the four-variable model, but it remains quantitatively reliable in predicting the period of the oscillations. Thus, the three-variable model, Eqs. (9), serves as a highly accurate approximation.

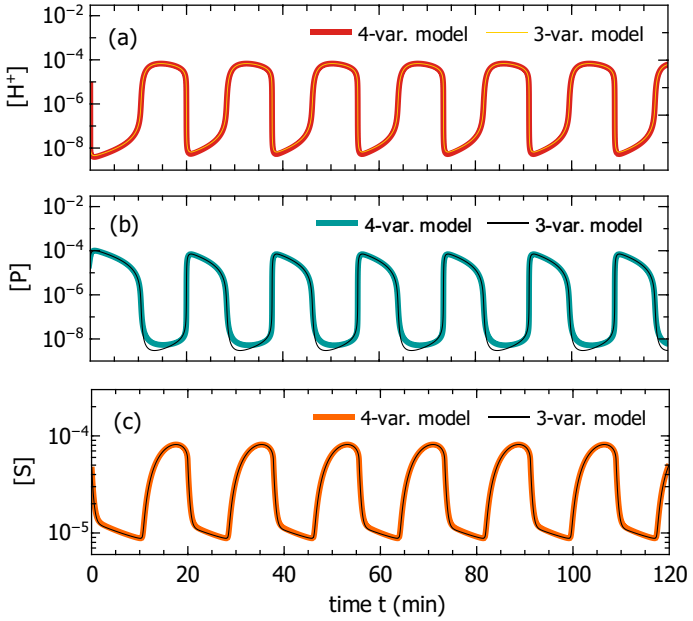

Figure 3: Comparison of predictions of the four- and three-variable models given by Eqs. (7) and (9), respectively. Evolution of concentrations describing acid $[H^+]$ (a), product [P] (b), and substrate [S] (c). The comparison of the corresponding pH is shown in Fig. 1f.

Reduced 2-variable model

The further reduction of Eqs. (9) to two species by means of an QSSA for [P] appears less accurate as the elimination of $[PH^+]$. Instead, we shall put forward a more appealing solution, which is essentially exact. For clarity, we switch to dimensionless variables $s(t) := [S](t)/[S_{ext}]$, $h(t) := [H^+](t)/[H^+_{ext}]$, and $p(t) = k'\,[P](t)$. With this, Eq. (8) yields the constraint $p(t)\,h(t) = [PH^+]/[H^+_{ext}] = \text{const}$, and thus

$$p(t)\frac{dh(t)}{dt} + \frac{dp(t)}{dt}h(t) = 0\,, \tag{11}$$

which implies that the dynamics of $p(t)$ and $h(t)$ are tightly coupled. After substitution of the time derivatives using Eqs. (9b) and (9c), the constraint assumes the form of a quadratic equation in $p = p(s,h)$,

$$p^2 + b(h)p - c(s,h) = 0\,, \tag{12}$$

with the dimensionless coefficients

$$b(h) = 1 + k'[H^+_{ext}]\,h + (1 - h^{-1})\,k_H/k \tag{13}$$

and

$$c(s,h) = \frac{2k'k_{cat}(s,h)[S_{ext}]}{k}\,s \geq 0\,. \tag{14}$$

Equation (12) possesses two roots, $p_\pm = (-b \pm \sqrt{b^2 + 4c})/2$, and selecting the positive solution, $p(s,h) \geq 0$ for all $s, h \geq 0$, we obtain

$$p(s,h) = \begin{cases} p_+(s,h), & \text{if } b(h) \geq 0\,, \\ p_-(s,h), & \text{if } b(h) < 0\,. \end{cases} \tag{15}$$

In particular, the time evolution of the rescaled concentration [P] of products is enslaved to the evolution of [S] and [H^+] and is given by $p(t) = p(s(t), h(t))$.

This solution for $p(t)$ allows us to eliminate [P] as a variable from the three-variable model in Eqs. (9). In particular, one verifies that Eq. (9c) is automatically satisfied and can be dropped. Casting the remaining Eqs. (9a) and (9b) in dimensionless form yields the two-variable model:

$$\frac{ds}{dt} = F(s,h) := -k_{\mathrm{cat}}(s,h)s + k_{\mathrm{S}}(1-s)\,, \tag{16a}$$

$$\frac{dh}{dt} = G(s,h) := -kp(s,h)h + k_{\mathrm{H}}(1-h)\,, \tag{16b}$$

where $p(s,h)$ is defined by relation (15) with the coefficients $b(s,h)$ and $c(s,h)$ given by Eqs. (13) and (14). We stress that Eq. (15) is an immediate consequence of Eq. (8), without further approximations. The two-variable model [Eqs. (16) with Eq. (15)] is thus an exact representation of the three-variable model (9). However, differently from the latter, Eqs. (16) do not have a meaningful interpretation as rate equations of a system of effective reactions unless one accepts $kp(s,h)$ as an effective decay rate of H^+. Since the introduction of nonelementary rates as a result of reduction on the deterministic level may lead to significant quantitative and even qualitative errors in stochastic simulations,[21,22] it is favorable to use the three-variable alternative as a stochastic model.

Fig. 4 shows the three-dimensional phase plot for the corresponding variables [S], [H^+], and [P] using different scales. It highlights two important features of the system. First, it becomes evident that the representation using the linear scales does not resolve well the structure of the limit cycle, especially at small concentrations of [H^+] (high pH). This suggests to utilize the logarithmic scales, which represents the structure of the limit cycle uniformly well in the whole range of values. This observation indicates that the behavior of the system differs from conventional examples of pH oscillators.[2] Second, the figure stresses the importance of the constraining manifold, which renders the three-dimensional system

effectively a two-dimensional one. Despite the presence of three variables, the behavior of the system is strictly confined to a two-dimensional manifold of roughly hyperbolic shape in the representation via linear scales, but it simplifies approximately to a plane in the logarithmic representation. Furthermore, the fact the constraining manifold deviates strongly from a plane, e.g., at a constant value of [P], signifies clearly that the naive orthogonal projection of the phase flow to such a plane for elimination of [P] as a variable would be a poor approximation of the true dynamics; an issue we will expand on below.

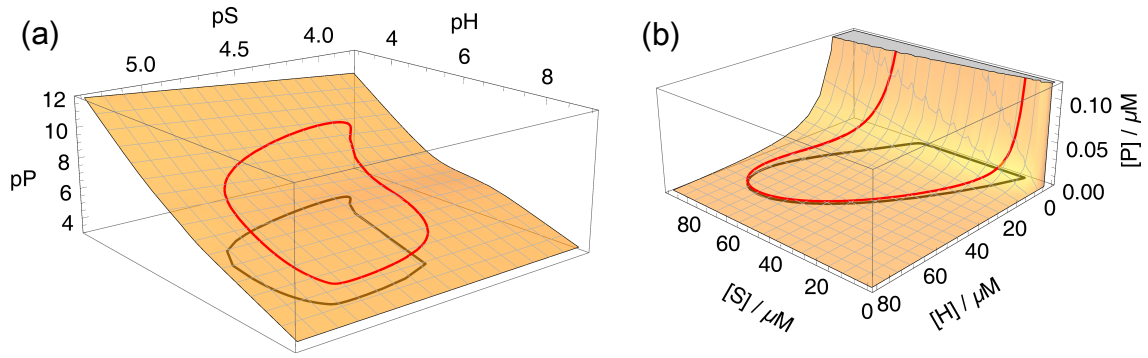

Figure 4: Phase plot of the limit cycle (red) of the three-variable model, Eq. (9), using logarithmic (a) and linear (b) scales. The surface is given by Eq. (15), which represents the constraint, Eq. (11). The black line is the orthogonal projection of the limit cycle to the plane $\mathrm{pP} = 4$ and $[\mathrm{P}] = 0$, respectively. In panel (a), we use the symbols $\mathrm{pX} = -\log_{10}([\mathrm{X}]/1\,\mathrm{M})$ for $X = \mathrm{S}, \mathrm{H}^+, \mathrm{P}$; note that small values of, e.g., pS correspond to large concentrations [S].

Limit cycle and structure of the phase flow

Nullclines

General properties of the limit cycle can be understood from the geometrics structure of the phase flow $(F(s,h), G(s,h))$ of a dynamic system. Helpful characteristics specifying the structure of the phase flow or phase portrait are nullclines. For the two-variable model (16), the S and H^+ nullclines are defined by the conditions $F(s,h) = 0$ and $G(s,h) = 0$, respectively. By construction, on a given nullcline the flow is perpendicular to the axis of the corresponding variable. The intersection of all nullclines defines all fixed points of the

phase flow, which represent the steady state solutions of Eqs. (16), i.e., the points where all time derivatives vanish. For the present two-variable model, both nullclines can be obtained analytically.

The S nullcline is calculated by putting $F(s,h) = 0$ in Eq. (16a), which on account of Eq. (2) leads to a quadratic equation in s:

$$s^2 + \beta(h)s - \bar{K}_\mathrm{M} = 0 \quad \text{with} \quad \beta(h) := \bar{K}_\mathrm{M} - 1 + \bar{v}_\mathrm{max} f_\mathrm{H}(h)\,, \tag{17}$$

where $\bar{v}_\mathrm{max} = v_\mathrm{max}/(k_\mathrm{S}[\mathrm{S}]_\mathrm{ext})$, $\bar{K}_\mathrm{M} = K_\mathrm{M}/[\mathrm{S}]_\mathrm{ext}$ and $f_\mathrm{H}(h)$ is given by Eq. (4). Out of the two roots $s_\pm(h)$, only the one describing non-negative substrate concentration is physically relevant, thus yielding the S nullcline,

$$s_\mathrm{S}^\mathrm{nc}(h) = s_+(h) := -\frac{\beta(h)}{2} + \frac{1}{2}\sqrt{\beta(h)^2 + 4\bar{K}_\mathrm{M}}\,. \tag{18}$$

To obtain the H^+ nullcline, we set $G(s,h) = 0$ in Eq. (16b) and, using the definition of $p(s,h)$, after some tedious algebra, we arrive at the intermediate relation,

$$2k' k_\mathrm{cat}(s,h)[\mathrm{S}]_\mathrm{ext} s = k_\mathrm{H}(h^{-1} - 1)(1 + k'[\mathrm{H}^+]_\mathrm{ext} h)\,. \tag{19}$$

More straightforwardly, we can derive this result by making use of Eq. (11), which implies that $dh/dt = 0$ is equivalent to $dp/dt = 0$ for $p(t), h(t) > 0$: set to zero the time derivative in Eq. (9c), solve for

$$kp(s,h) = \frac{2k' k_\mathrm{cat}(s,h)[\mathrm{S}]_\mathrm{ext}}{1 + k'[\mathrm{H}^+]_\mathrm{ext} h}\, s\,, \tag{20}$$

and substitute it in Eq. (16b). Finally, inserting the definition of $k_\mathrm{cat}(s,h)$, Eq. (2), into the intermediate equation for s leads us to the H^+ nullcline,

$$s_\mathrm{H}^\mathrm{nc}(h) = \bar{K}_\mathrm{M} \left[\frac{2k' v_\mathrm{max} f_\mathrm{H}(h)}{k_\mathrm{H}(h^{-1} - 1)(1 + k'[\mathrm{H}^+]_\mathrm{ext} h)} - 1\right]^{-1}\,. \tag{21}$$

Phase flow

The origin of the limit cycle is easily understood from the phase portrait of the two-dimensional dynamical system, Eqs. (16), and the associated nullclines, Eqs. (18) and (21). As mentioned earlier, a remarkable feature of this system is that the structure of the phase flow is best unveiled on logarithmic scales—in contrast to conventional examples of oscillators. Therefore, instead of the original variables s and h, we will use $\mathrm{pS} = -\log_{10}(s[\mathrm{S}]_{\mathrm{ext}}/1\,\mathrm{M})$ and pH as axes of the phase plane. The phase flow of the two-variable model together with its nullclines and the limit cycle are shown in Fig. 5a. For the parameters considered here, the nullclines intersect only in a single, repelling fixed point enclosed by the limit cycle. The limit cycle was obtained from the numerical solution of $ds/dt = F(s,h)$ and $dh/dt = G(s,h)$ after a sufficiently long initial relaxation time.

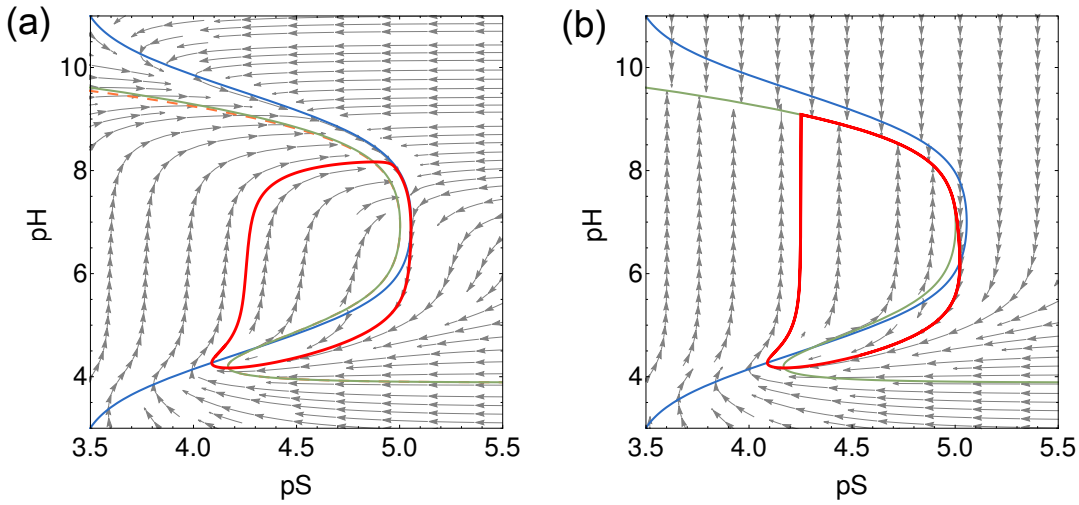

Figure 5: Phase flows and limit cycles in the pS-pH plane. Comparison of two two-variable models reduced from the three-variable model, Eq. (9), by different elimination of the product. The S (blue line) and H^+ (green line) nullclines are the same for both models and are given by Eqs. (18) and (21), respectively. (a): Model obtained by the exact elimination of product p, see Eq. (16). (b): Model obtained by imposing QSSA for the variable p, as given by Eq. (23).

Qualitatively, the shape of the limit cycle is determined by the nullclines and the two-dimensional flow field $(F(s,h), G(s,h))$. The S nullcline (Eq. (18), blue line) has a rotated bell shape and the H^+ nullcline (Eq. (21), green line) is of a reversed s-like shape. The

requirement on the flow field that, at any point of the nullclines, there is no motion along the corresponding direction means that the flow on the S nullcline can only point along the pH direction (vertical arrows) and on the H^+ nullcline along the pS direction (horizontal arrows). In the high pH regime, both nullclines run closely together such that the H^+ nullcline pushes the flow towards the S nullcline. This causes a channeling of the flow between the two nullclines towards the apex of the S nullcline, where $s_S^{nc}(h)$ attains its maximum value (pS $\approx$ 5.0). There, the flow points downwards, along the pH axis, and is tightly restricted with respect to pS (i.e., horizontally), concomitantly the pH value drops rapidly. All phase trajectories, irrespective of their starting point, eventually approach this apex point arbitrarily closely and follow the S nullcline for a moment, which essentially defines a piece of the limiting trajectory (limit cycle, red line). After this point, the S nullcline bends away from the vertical, but the trajectory keeps following the flow field and revolves around the fixed point until the orbit closes, which forms the limit cycle. Thus, the limit cycle is determined as the trajectory that starts in the apex of the S nullcline, where the curve attains its largest pS value.

Failure of QSSA for P

In the literature, it was suggested to apply the quasi-steady state approximation (QSSA) to the concentration [P] of products.[16,17] Here we elaborate on the consequences of this approximation and show that although the nullclines remain the same as in the exact reduction scheme, it qualitatively changes the phase flow. In hindsight, it is clear that such an approximation cannot be consistent with the QSSA for PH^+, which leads to the three-variable model, Eqs. (10), and constrains the three-dimensional flow to a two-dimensional manifold as discussed above (Fig. 4).

This elimination scheme follows directly from Eqs. (9) by enforcing the QSSA for p. Setting $dp/dt = 0$ in Eq. (9c) and proceeding to dimensionless variables, $u(h) = 1 +$

$(k'[\mathrm{H}^+]_{\mathrm{ext}}h)^{-1}$ and $r_{\mathrm{e}} = [\mathrm{S}]_{\mathrm{ext}}/[\mathrm{H}^+]_{\mathrm{ext}}$, we find

$$kp(s,h)h = 2r_{\mathrm{e}}k_{\mathrm{cat}}(s,h)s/u(h)\,. \tag{22}$$

Finally, substituting the combination $kp(s,h)h$ in Eq. (9b), we arrive at the model:

$$\frac{ds}{dt} = -k_{\mathrm{cat}}(s,h)s + k_{\mathrm{S}}(1-s)\,, \tag{23a}$$

$$\frac{dh}{dt} = -2r_{\mathrm{e}}k_{\mathrm{cat}}(s,h)s\,u(h)^{-1} + k_{\mathrm{H}}(1-h)\,. \tag{23b}$$

In our previous study,[17] this model was used with $u(h) = 1$ to qualitatively obtain the structure of the phase portrait exhibited by the numerical solution of the four-variable model. As earlier, the H^+ nullcline corresponding to Eq. (23b) follows simply by setting $dh/dt = dp/dt = 0$ in Eqs. (9b) and (9c) and solving for $s(h)$. Expressing the combination kph from the equation for h and equating it with that from Eq. (22), we end up with the H^+ nullcline identical to Eq. (21). The S nullcline is given by Eq. (18) due to the coincidence of the equations for s, cf. Eq. (16a) and Eq. (23a).

By comparing the phase plots of the models given by Eq. (16) and Eq. (23), cf. Fig. 5a and Fig. 5b, we can immediately notice that although the nullclines of both models are the same, the flow fields in the upper half of the plots (larger pH) are drastically different. In particular, the behavior of the flow field on the upper branch of the H^+ nullcline described by model Eq. (23) becomes degenerate, Fig. 5b. Indeed, by construction, the arrows have to be horizontal on the H^+ nullcline, meaning the absence of the vertical component of the flow field. Although this requirement remains fulfilled, the horizontal component of the flow also turns to zero. Moreover, a close inspection of Fig. 5b reveals that the structure of the limit cycle becomes qualitatively different. In contrast to the accurate scenario shown in Fig. 5a, the shape of the limit cycle is now fully set by the upper branch of the H^+ nullcline, which directly affects the period of oscillation predicted by this model.

We note that the model given by Eq. (23), and hence the QSSA for the product P,

correspond to a special limit of the model given by Eq. (16). It follows from the exact solution for p, see Eqs. (13)−(15), in the limit $b^2 \gg 4c$ with b dominated by the contribution $b \approx 1 + k'[\mathrm{H}^+] = k'h[\mathrm{H}^+]_{\mathrm{ext}}u(h) > 0$ yielding $p = p_+ \approx [-b + b(1 + 2c/b^2)]/2 = c/b = 2r_{\mathrm{e}}k_{\mathrm{cat}}(s,h)s[khu(h)]^{-1}$, cf. Eq. (9c) for $dp/dt = 0$. The requirement $b > 0$ is imposed by the necessary condition that the concentration $p(t)$ remains always non-negative and implies that $k'h[\mathrm{H}^+]_{\mathrm{ext}}u(h) \gg k_{\mathrm{H}}(1 - h^{-1})/k$. The latter is justified for a part of the time period only, when h is large enough (low pH). For the rest of the period, when h is relatively small (high pH), the more accurate solution for $p(t)$ is governed by the case $b < 0$ and is defined by the root p_-. Therefore, disregarding this root in favor of p_+ for all times is the reason that significantly restricts the validity of the QSSA for P and the whole model given by Eq. (16). This reasoning explains why the model given by Eq. (23) causes the degeneracy and becomes unreliable in the domain of high pH.

Finally, as can be seen from Fig. 5a and Fig. 5b, the S and H^+ nullclines exhibit a single intersection, with the neighboring flow field indicating existence of an unstable fixed point. Note that in the vicinity of the fixed point models given by Eq. (16) and Eq. (23) display very similar flow fields, see Fig. 6. This is not unexpected because the exact model Eq. (16) admits formal reduction to the approximate model Eq. (23) in the domain of relatively small pH. For the given parameters, the fixed point is found to take place at $(\mathrm{pS}_*, \mathrm{pH}_*) \approx (4.31, 4.57)$, which is fully consistent with the earlier finding.[17] By linearizing the system around this fixed point, we find that the unsteady equilibrium corresponds to an unstable focus, which serves as a repeller. On account of the discussed properties of the nullclines and phase flow, we conclude that the phase trajectory is forced to form a closed orbit around the repeller, which constitutes the limit cycle and completes our analysis.

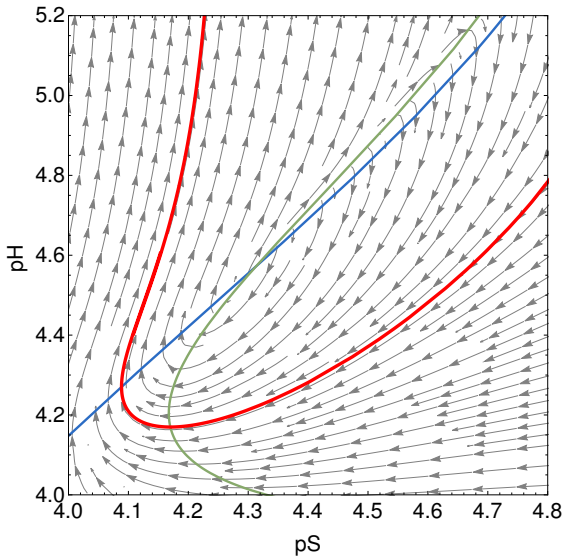

Figure 6: Close-up of the phase portrait in Fig. 5 in the vicinity of the fixed point. The red line shows a part of the limit cycle, and gray arrows indicate the phase flow. The fixed point is given as the intersection of the S nullcline (blue line, Eq. (18)) and the H^+ nullcline (green line, Eq. (21)). Note that in the shown regime of relatively small pH, the behavior of the two models Eq. (16) and Eq. (23) is similar.

Summary and conclusions

We have theoretically studied an urea-urease-based pH oscillator confined to a giant lipid vesicle, which is capable of differential transport of urea and hydrogen ion across the unilamellar membrane and serves as an open reactor. In contrast to conventional pH oscillators in closed chambers, the exchange with the vesicle exterior periodically resets the pH clock that switches the system from acid to basic. Here, we have focused on large vesicles of sizes of several micrometers, which justifies a deterministic treatment of the dynamics. Quite importantly, as shown recently by a stochastic simulation study,[17] the structure of the limit cycle of the deterministic rate equations controls not only the behavior for giant vesicles, but also dominates the pronouncedly stochastic oscillations in vesicles of submicrometer size. This justifies our deterministic approach and prompts the analysis of the structure of the phase flow and the limit cycle.

Starting from a reaction scheme involving four species, namely urea as the substrate S, hydrogen ion H^+, ammonia as product P, and ammonium as its ion form PH^+, we have

obtained accurate reduced models by eliminating the product species. We have first reduced the system of rate equations to three variables by excluding PH^+ via a quasi-steady state assumption (QSSA). Next, we have eliminated P to arrive at a model for two variables S and H^+ that is an *exact* representation of the three variable model. In particular, we have shown that the QSSA for PH^+ in the first step introduces a constraint that couples the dynamics of H^+ and P, implying that the three-variable model is effectively a two dimensional one. The constraint manifests itself as a nontrivial manifold that restricts the phase flow and the limit cycle to live in. The structure of the phase flow and the properties of the limit cycle are best uncovered using a logarithmic representation—in contrast to conventional examples of oscillators.

By analyzing the phase flow and mutual positioning of nullclines, we have shown that the limit cycle is set by the S nullcline. Noteworthy, this outcome is in contrast to our expectations based on the QSSA for P from an earlier study,[17] which suggested that the limit cycle is set by the H^+ nullcline. However, already a quick inspection of a three-dimensional phase plot (Fig. 4), where the concentration of P varies by four orders of magnitude and the constraining manifold is drastically different from a plane, indicated that this reduction scheme does not appear as a good idea. We have further demonstrated that the QSSA for P approximates the full model only in the acid regime (low pH) and leads to degenerate behavior of the flow field near the high-pH branch of the H^+ nullcline. Even though the nullclines remain identical for both two-dimensional models, the structure of the phase flow is different, in particular, in the basic regime. Moreover, the QSSA for P is mathematically unjustified and leads to inconsistencies in the regime of high pH. Thus, the quality of the model and the accuracy of its predictions, including the oscillation period, are highly sensitive to the choice of the reduction scheme.

An important advantage of our findings is that whereas the two-variable model is more amendable to analytic treatments, its three-dimensional counterpart admits a reliable interpretation as a reaction scheme and is favorable for stochastic simulations. These models

can be used for accurate descriptions of pH oscillations in giant, but also small vesicles; for the latter, correctly reproducing the oscillation periods is vital for the comparison with experimental conditions and for rationalizing experiments. Furthermore, a faithful model of a single pH oscillator is a crucial prerequisite for understanding communication of vesicles and synchronization of rhythms.[10,23–25]

Acknowledgement

This research has been supported by Deutsche Forschungsgemeinschaft (DFG) through grant SFB 1114, project no. 235221301 (sub-project C03) and under Germany's Excellence Strategy – MATH+ : The Berlin Mathematics Research Center (EXC-2046/1) – project no. 390685689 (subproject AA1-1).

References

(1) Novák, B.; Tyson, J. J. Design Principles of Biochemical Oscillators. *Nat. Rev. Mol. Cell Biol.* **2008**, *9*, 981–991.

(2) Orbán, M.; Kurin-Csörgei, K.; Epstein, I. R. pH-Regulated Chemical Oscillators. *Acc. Chem. Res.* **2015**, *48*, 593–601.

(3) Cupić, Ž. D.; Taylor, A. F.; Horváth, D.; Orlik, M.; Epstein, I. R. Editorial: Advances in Oscillating Reactions. *Front. Chem.* **2021**, *9*, 690699.

(4) Zhang, Y.; Sun, C.; Wang, C.; Jankovic, K. E.; Dong, Y. Lipids and Lipid Derivatives for RNA Delivery. *Chem. Rev.* **2021**, *121*, 12181 – 12277.

(5) Alberty, R. A.; Massey, V. On the Interpretation of the pH Variation of the Maximum Initial Velocity of an Enzyme-Catalyzed Reaction. *Biochim. Biophys. Acta* **1954**, *13*, 347–353.

(6) Hu, G.; Pojman, J. A.; Scott, S. K.; Wrobel, M. M.; Taylor, A. F. Base-Catalyzed Feedback in the Urea-Urease Reaction. *J. Phys. Chem. B* **2010**, *114*, 14059–14063.

(7) Muzika, F.; Růžička, M.; Schreiberová, L.; Schreiber, I. Oscillations of pH in the Urea–Urease System in a Membrane Reactor. *Phys. Chem. Chem. Phys.* **2019**, *21*, 8619–8622.

(8) Miele, Y.; Bánsági, T.; Taylor, A. F.; Stano, P.; Rossi, F. Engineering Enzyme-Driven Dynamic Behaviour in Lipid Vesicles. Advances in Artificial Life, Evolutionary Computation and Systems Chemistry. Cham, 2016; pp 197–208.

(9) Miele, Y.; Bánsági, T.; Taylor, A. F.; Rossi, F. Modelling Approach to Enzymatic pH Oscillators in Giant Lipid Vesicles. Adv. Bionanomater.: Lecture Notes in Bioengineering. Cham, 2018; pp 63–74.

(10) Miele, Y.; Jones, S. J.; Rossi, F.; Beales, P. A.; Taylor, A. F. Collective Behavior of Urease pH Clocks in Nano- and Microvesicles Controlled by Fast Ammonia Transport. *The Journal of Physical Chemistry Letters* **2022**, *13*, 1979–1984.

(11) Krajewska, B. Ureases I. Functional, Catalytic and Kinetic Properties: A Review. *J. Mol. Catal. B: Enzym.* **2009**, *59*, 9–21.

(12) Qin, Y.; Cabral, J. M. S. Kinetic Studies of the Urease-Catalyzed Hydrolysis of Urea in a Buffer-Free System. *Appl. Biochem. Biotechnol.* **1994**, *49*, 217–240.

(13) Fidaleo, M.; Lavecchia, R. Kinetic Study of Enzymatic Urea Hydrolysis in the pH Range 4–9. *Chem. Biochem. Eng. Q.* **2003**, *17*, 311–318.

(14) Krajewska, B.; Ciurli, S. Jack Bean (Canavalia Ensiformis) Urease. Probing Acid–Base Groups of the Active Site by pH Variation. *Plant Physiol. Biochem.* **2005**, *43*, 651–658.

(15) Bubanja, I. N.; Bánsági, T.; Taylor, A. F. Kinetics of the Urea-Urease Clock Reaction

With Urease Immobilized in Hydrogel Beads. *React. Kinet. Mech. Catal.* **2018**, *123*, 177–185.

(16) Bánsági, T.; Taylor, A. F. Role of Differential Transport in an Oscillatory Enzyme Reaction. *J. Phys. Chem. B* **2014**, *118*, 6092–6097.

(17) Straube, A. V.; Winkelmann, S.; Schütte, C.; Höfling, F. Stochastic pH Oscillations in a Model of the Urea–Urease Reaction Confined to Lipid Vesicles. *J. Phys. Chem. Lett.* **2021**, *12*, 9888–9893.

(18) Eigen, M. Proton Transfer, Acid-Base Catalysis, and Enzymatic Hydrolysis. Part I: Elementary Processes. *Angew. Chem. Int. Ed. Engl.* **1964**, *3*, 1–19.

(19) Segel, L. A.; Slemrod, M. The Quasi-Steady-State Assumption: A Case Study in Perturbation. *SIAM Rev.* **1989**, *31*, 446–477.

(20) Wechselberger, M. *Geometric singular perturbation theory beyond the standard form*; Frontiers in Applied Dynamical Systems: Reviews and Tutorials; Springer: Cham, 2020; Vol. 6; p 137.

(21) Thomas, P.; Straube, A. V.; Grima, R. Stochastic Theory of Large-Scale Enzyme-Reaction Networks: Finite Copy Number Corrections to Rate Equation Models. *J. Chem. Phys.* **2010**, *133*, 195101.

(22) Thomas, P.; Straube, A. V.; Grima, R. The Slow-Scale Linear Noise Approximation: An Accurate, Reduced Stochastic Description of Biochemical Networks Under Timescale Separation Conditions. *BMC Syst. Biol.* **2012**, *6*, 39.

(23) Pikovsky, A.; Rosenblum, M.; Jürgen, K. *Synchronization a Universal Concept in Nonlinear Sciences*; Cambridge University Press: Cambridge, UK, 2001.

(24) Budroni, M. A.; Torbensen, K.; Ristori, S.; Abou-Hassan, A.; Rossi, F. Membrane

Structure Drives Synchronization Patterns in Arrays of Diffusively Coupled Self-Oscillating Droplets. *J. Phys. Chem. Lett.* **2020**, *11*, 2014–2020.

(25) Budroni, M. A.; Pagano, G.; Conte, D.; Paternoster, B.; D'ambrosio, R.; Ristori, S.; Abou-Hassan, A.; Rossi, F. Synchronization Scenarios Induced by Delayed Communication in Arrays of Diffusively Coupled Autonomous Chemical Oscillators. *Phys. Chem. Chem. Phys.* **2021**, *23*, 17606–17615.